Available online at www.sciencedirect.com
ScienceDirect
Trans. Nonferrous Met. Soc. China 24(2014) 1352−1364
Transactions of Nonferrous Metals Society of China
www.tnmsc.cn

Effect of Y addition on microstructure and mechanical properties of Mg−Zn−Mn alloy

Fu-gang QI[1], Ding-fei ZHANG[2], Xiao-hua ZHANG[1], Fu-sheng PAN[2]

1. Science and Technology on Surface Physics and Chemistry Laboratory, China Academy of Engineering Physics, Mianyang 621907, China;
2. College of Materials Science and Engineering, Chongqing University, Chongqing 400045, China

Received 9 June 2013; accepted 9 August 2013

Abstract: The effects of Y on the microstructure and mechanical properties of Mg−6Zn−1Mn alloy were investigated. The results show that the addition of Y has significant effect on the phase composition, microstructure and mechanical properties of Mg−6Zn−1Mn alloy. Varied phases compositions, including Mg_7Zn_3, *I*-phase (Mg_3YZn_6), *W*-phase ($Mg_3Y_2Zn_3$) and *X*-phase ($Mg_{12}YZn$), are obtained by adjusting the Zn to Y mass ratio. Mn element exists as the fine Mn particles, which are well distributed in the alloy. Thermal analysis and microstructure observation reveal that the phase stability follows the trend of *X*>*W*>*I*>Mg_7Zn_3. In addition, Y can improve the mechanical properties of Mg−Zn−Mn alloy significantly, and the alloy with Y content of 6.09% has the best mechanical properties. The high strength is mainly due to the strengthening by the grain size refinement, dispersion strengthening by fine Mn particles, and introduction of the Mg−Zn−Y ternary phases.
Key words: Mg−Zn−Mn alloy; Y; microstructure; mechanical property; fracture

1 Introduction

As the lightest metallic structure materials, magnesium alloys have great potential for the aerospace, transportation and mobile electronic industries due to their high specific strength and stiffness, good damping capacity, excellent machinability and good castability [1−3]. However, the application of magnesium alloys is still limited due to low strength and poor formability [4,5]. Therefore, the wide application of magnesium alloys depends heavily on the development of new high-strength wrought magnesium alloys.

Recently, ZHANG et al [6,7] have developed a high-strength Mg−6Zn−1Mn (ZM61) wrought alloy. The alloy with solution treatment and double aging treatment (high temperature aging after pre-aging at a lower temperature) exhibits the tensile strength of 366 MPa, yield strength of 340 MPa and elongation of 6.3% at room temperature. The superior mechanical properties of this alloy are mainly due to the precipitation strengthening by the $MgZn_2$ precipitates. However, the complex heat treatment process is not practical for industrial application. Therefore, in order to further improve the mechanical properties of the extruded ZM61 alloy, a modification in composition is necessarily made by adding alloy elements.

It is well known that the addition of rare earth elements to magnesium alloys is an effective way to refine grain, improve the mechanical properties at ambient and elevated temperatures, and improve the casting characteristics [8−12]. Among them, Y has received a particular attention. In recent years, it has been reported that Y element can form several secondary phases in Mg−Zn alloys [11,13,14], and has a favorable effects on the mechanical properties [2,9,10,15−17]. In addition, it was reported that the addition of Mn has the function of refining grain size and improving tensile strengths of Mg−Al−Zn system alloys [18]. Recently, the microstructure and mechanical properties of Mg−Zn−Mn alloys with various Mn contents have been investigated [19]. According to that, the extruded alloy with about 1% Mn exhibits the optimal tensile properties because of refining the grain size. But up to now, little research has

Foundation item: Project (2007CB613700) supported by the National Basic Research Program of China; Project(2011BAE22B01-3) supported by the National Key Technologies R&D Program of China; Project (2010DFR50010, 2008DFR50040) supported by the International Scientific and Technological Cooperation Program of Ministry of Science and Technology of China; Project (CSTC, 2010AA4048) supported by Chongqing Science and Technology Commission, China
Corresponding author: Fu-gang QI; Tel: +86-816-3626782; E-mail: fugangqi@gmail.com
DOI: 10.1016/S1003-6326(14)63199-X

been carried out on the microstructure and mechanical properties of Mg−Zn− Mn−Y alloy.

In the present study, the effects of Y on the microstructure and mechanical properties of Mg−6Zn−1Mn alloy are studied in order to provide a reference for the development of new rare earth-containing magnesium alloy.

2 Experimental

The experimental alloys were prepared from commercial high-purity Mg (>99.9%, wt.%) and Zn (>99.95%), Mg−4.1%Mn and Mg−30.29%Y master alloys. All the materials were melted in a ZG−0.01 vacuum induction melting furnace at about 730 °C under an Ar atmosphere. The actual chemical compositions of the experimental alloy ingots were analyzed by XRF−800 CCDE X-ray fluorescence spectrometer and the results are listed in Table 1. The cylinder-shaped ingots were homogenized at 400 °C for 16 h and then air cooled. To investigate the effect of the temperature on the phase stability, small samples of as-cast alloys III and V for microstructure observation were homogenized at 500 °C for 16 h and then cooled in air. Before the ingots were extruded, both the alloy ingots and extrusion die were heated to 450 °C for 60 min. Then the ingots were hot extruded into rods with the diameter of 16 mm at 450 °C with a ratio of 25:1. Extrusion was conducted under a controlled constant force by an XJ-500 horizontal extrusion machine. After extrusion, the extrusion bars were cooled in open air.

Table 1 Chemical composition of test alloys (mass fraction, %)

Alloy No.	Nominal composition	Actual composition			
		Zn	Mn	Y	Mg
I	Mg−6Zn−1Mn	5.62	0.72	0	Bal.
II	Mg−6Zn−1Mn−0.7Y	5.95	0.96	0.71	Bal.
III	Mg−6Zn−1Mn−2Y	5.74	0.79	1.83	Bal.
IV	Mg−6Zn−1Mn−3Y	5.89	0.77	3.02	Bal.
V	Mg−6Zn−1Mn−6Y	5.66	0.92	6.09	Bal.

Cylindrical tensile samples of 60 mm in gauge length and 5 mm in gauge diameter were machined from as-extruded bars for tensile tests at ambient temperature. Tensile tests were conducted with a constant displacement rate of 3 mm/min on a SANS CMT−5105 electronic universal testing machine. Mechanical properties were determined from a complete stress−strain curve. 0.2% yield strength (YS), ultimate tensile strength (UTS) and fracture elongation (elongation) were obtained based on the average of three tests.

The microstructure of the specimens was examined using a NEISS NEOPHOT−30 optical microscope (OM). The microstructural morphology and compound composition of the alloys were examined by a TESCAN VEGA Ⅱ scanning electron microscope (SEM) equipped with an Oxford INCA Energy 350 energy dispersive X-ray spectrometer (EDS) and a Zeiss LIBRA 200 FE transmission electrical microscope (TEM) operating at 200 kV. Phase analysis was determined by a Rigaku D/max 2500PC X-ray diffractometer (XRD) using a Cu K_α radiation with a scanning angle from 10° to 90 ° and a scanning rate of 4 (°)/min. Fracture surface was investigated by using secondary electron (SE) imaging and backscatter electron (BSE) imaging.

Thermal analysis was performed using a differential scanning calorimeter (DSC, a NETZSCH STA 449C system). Specimens for thermal measurements with 3 mm in diameter were cut from as-cast ingots. Then they were cut to a final mass of about 10 mg. Thermal scanning of each sample was carried out in the temperature range of 50−700 °C with both cooling and heating profiles under flowing Ar. The heating curve was obtained by heating the sample hermetically up to 700 °C at a heating rate of 10 °C/min followed by cooling down to 50 °C at 10 °C/min to obtain the cooling curve.

3 Results and discussion

3.1 Microstructure of as-cast alloys

The as-cast microstructures of the investigated alloys are indicative of structural refinement in the Mg−6Zn−1Mn alloy after Y addition, as shown in Fig. 1. It can be preferred that Y element has effect on grain refinement of as-cast Mg−Zn−Mn−Y alloys. Figure 2 shows the X-ray diffraction patterns of as-cast Mg−Zn−Mn−Y alloys. With the variation of Y content, the main phases of the experiment alloys will change as shown in Fig. 2 and Table 2. For the Y-free based alloy (alloy I), the main phases are the α-Mg matrix, Mn and Mg_7Zn_3 phases. Figure 3(a) shows the SEM microstructure of alloy I. The second phases distributing at the interdendritic consist of Mg, Zn and Mn elements and the atomic ratio of Mg to Zn is about 7:3 according to EDS analysis. It can be inferred that the second phase is mainly Mg_7Zn_3 phase. When Y content increases to 0.71% (alloy Ⅱ), a little amount of *I*-phase (Mg_3YZn_6, icosahedral quasicrystal structure, quasi-periodically ordered) as well as a large amount of α-Mg matrix is observed, as shown in Fig. 2. Figure 3(b) displays the SEM image of the *I*-phase/α-Mg matrix eutectic pockets in alloy II. When the Y content varies from 0.71% to 1.83% (alloy III), *W*-phase ($Mg_3Y_2Zn_3$, cubic structure) is also detected by XRD as well as *I*-phase and α-Mg.

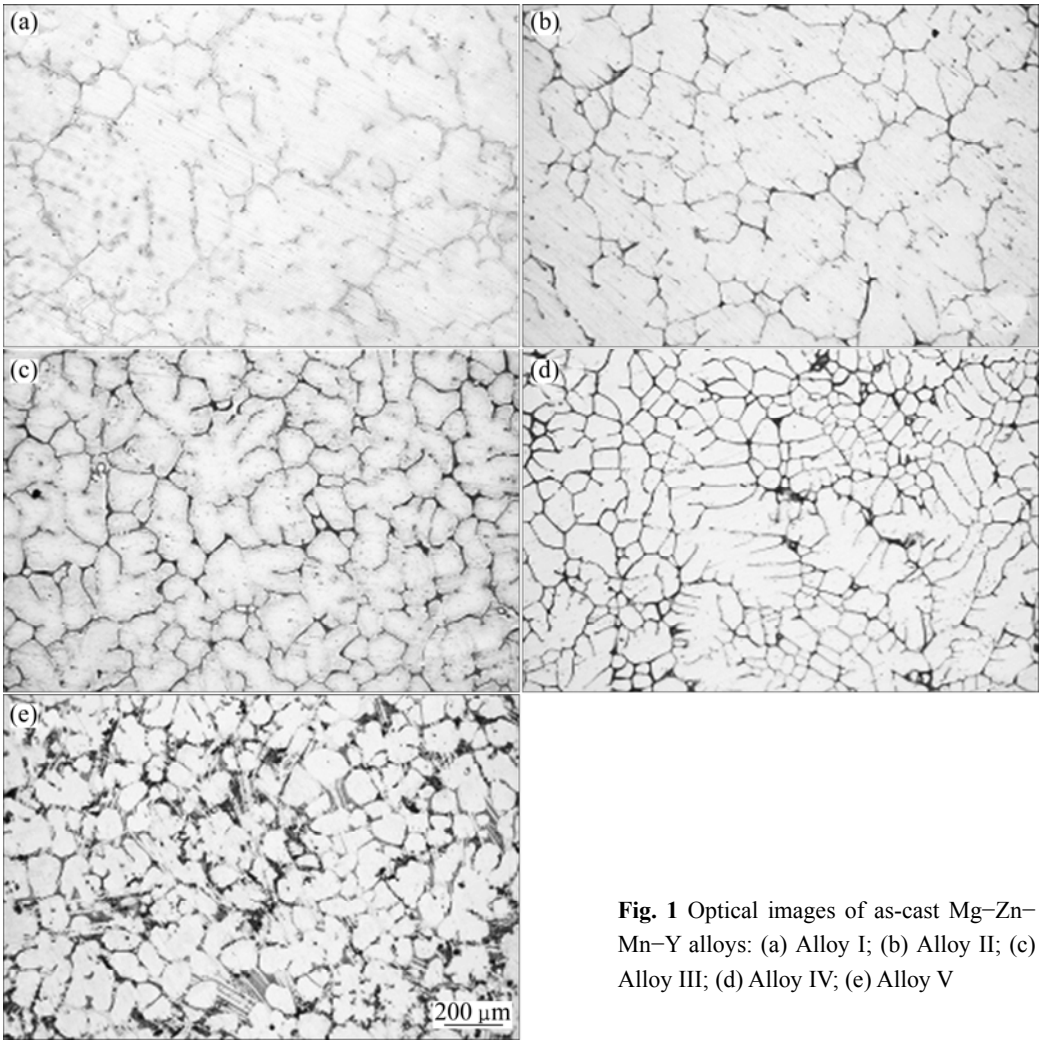

Fig. 1 Optical images of as-cast Mg−Zn−Mn−Y alloys: (a) Alloy I; (b) Alloy II; (c) Alloy III; (d) Alloy IV; (e) Alloy V

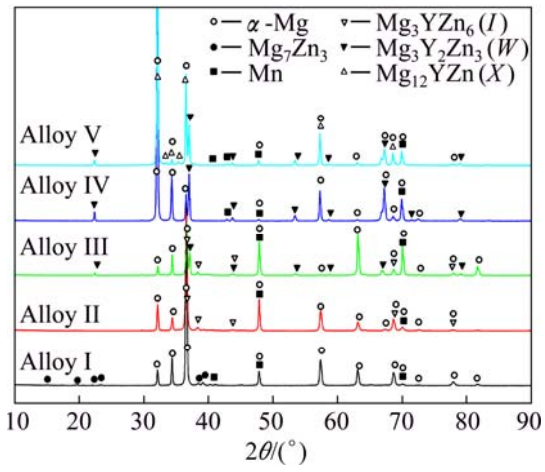

Fig. 2 XRD patterns of as-cast Mg−Zn−Mn−Y alloys

The microstructure of alloy III is shown in Fig. 3(c). The secondary phases including *I*-phase and *W*-phase distribute mainly at the triangle and intergranular grain boundary [16]. The morphologies of *W*-phase and *I*-phase are lamellar. When Y content is 3.2% (alloy IV), *W*-phase becomes the main phase while no *I*-phase can be detected within the sensitivity limit of X-ray diffraction. The SEM image of alloy IV shown in Fig. 3(d) reveals that the *W*-phase mainly exists at the triangle grain boundary. With the further increase of Y content (alloy V), the diffraction peak of *X*-phase ($Mg_{12}YZn$, long period stacking ordered (LPSO) structure) can be detected and the main phases are *α*-Mg, Mn, *W*-phase and *X*-phase. Figure 3(e) shows a SEM image of alloy V. The *W*-phase and *X*-phase alternately grow during the solidification process, resulting in good combination of two phases as shown in Fig. 3(e).

To further illustrate the existence form and distribution of Mn element in as-cast test alloys, high-

Table 2 Summary of main phases for Mg−Zn−Mn−Y alloy

Alloy No.	m(Zn)/m(Y)	Main phase
I	—	*α*-Mg, Mn and Mg_7Zn_3
II	8.38	*α*-Mg, Mn and *I*-phase
III	3.13	*α*-Mg, Mn, *I*-phase and *W*-phase
IV	1.95	*α*-Mg, Mn and *W*-phase
V	0.93	*α*-Mg, Mn, *W*-phase and *X*-phase

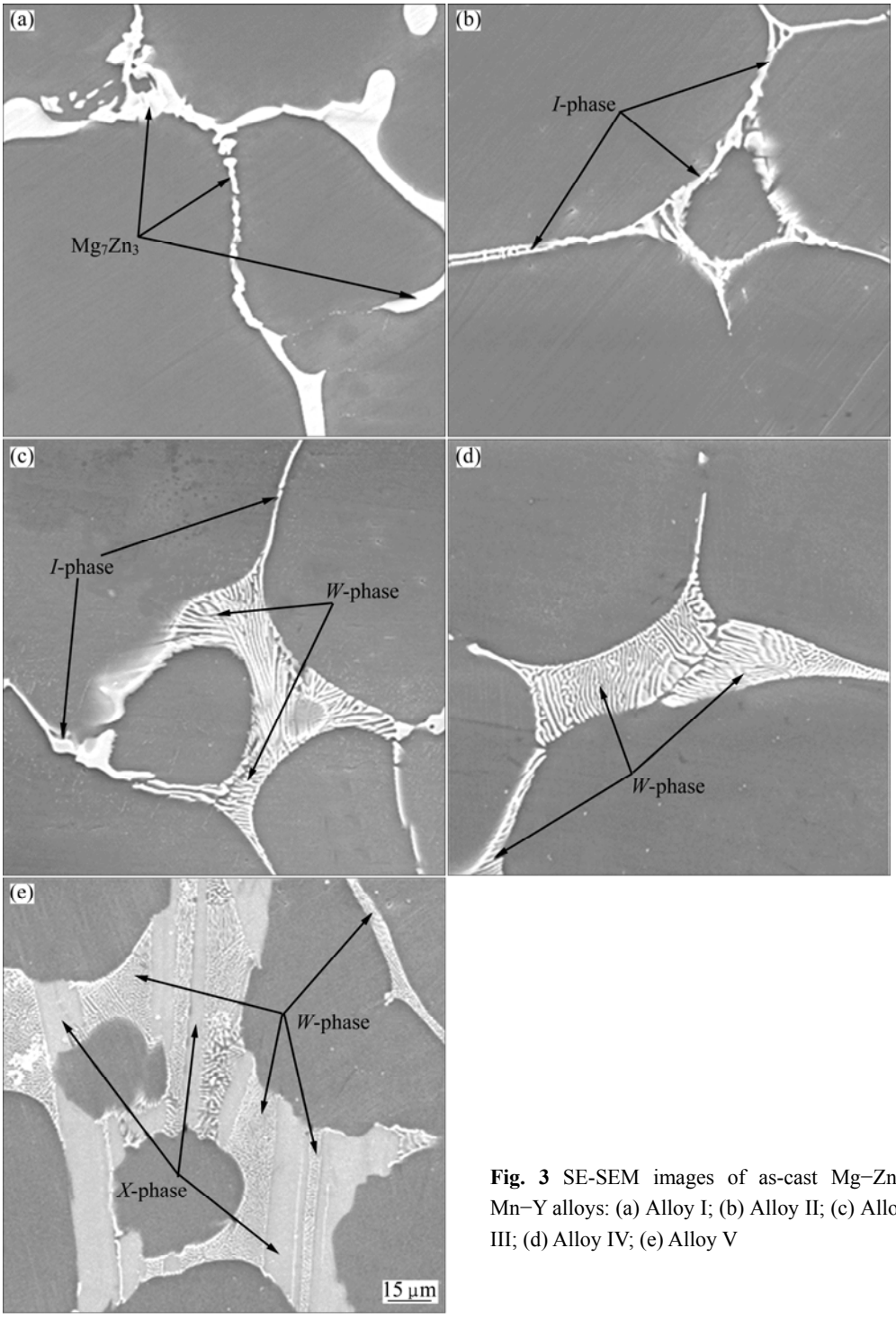

Fig. 3 SE-SEM images of as-cast Mg−Zn−Mn−Y alloys: (a) Alloy I; (b) Alloy II; (c) Alloy III; (d) Alloy IV; (e) Alloy V

magnification microstructure observation with EDS analysis was carried out. Figure 4 and Table 3 show the high-magnification SEM image and EDS analysis of as-cast alloy III. There are four main phases in this alloy: α-Mg matrix, Mn, *I*-phase and *W*-phase. The EDS spot analysis results reveal that Mn is evenly dispersed in α-Mg matrix and secondary phases. Analyses of EDS line scanning (Fig. 4(b)) further confirm the uniform distribution of Mn element. In addition, the distribution of elements Mg, Zn, Mn and Y for the studied alloy III (Figs. 4(d)−(h)) can also further confirm the dispersion of Mn.

3.2 Phase stability

Figure 5 shows the optical microstructures of as-homogenized Mg−Zn−Mn−Y alloys. It is well known that the melting temperature of Mg−Zn phase is about 340 °C [9,20]. Therefore, for the alloy I without Y,

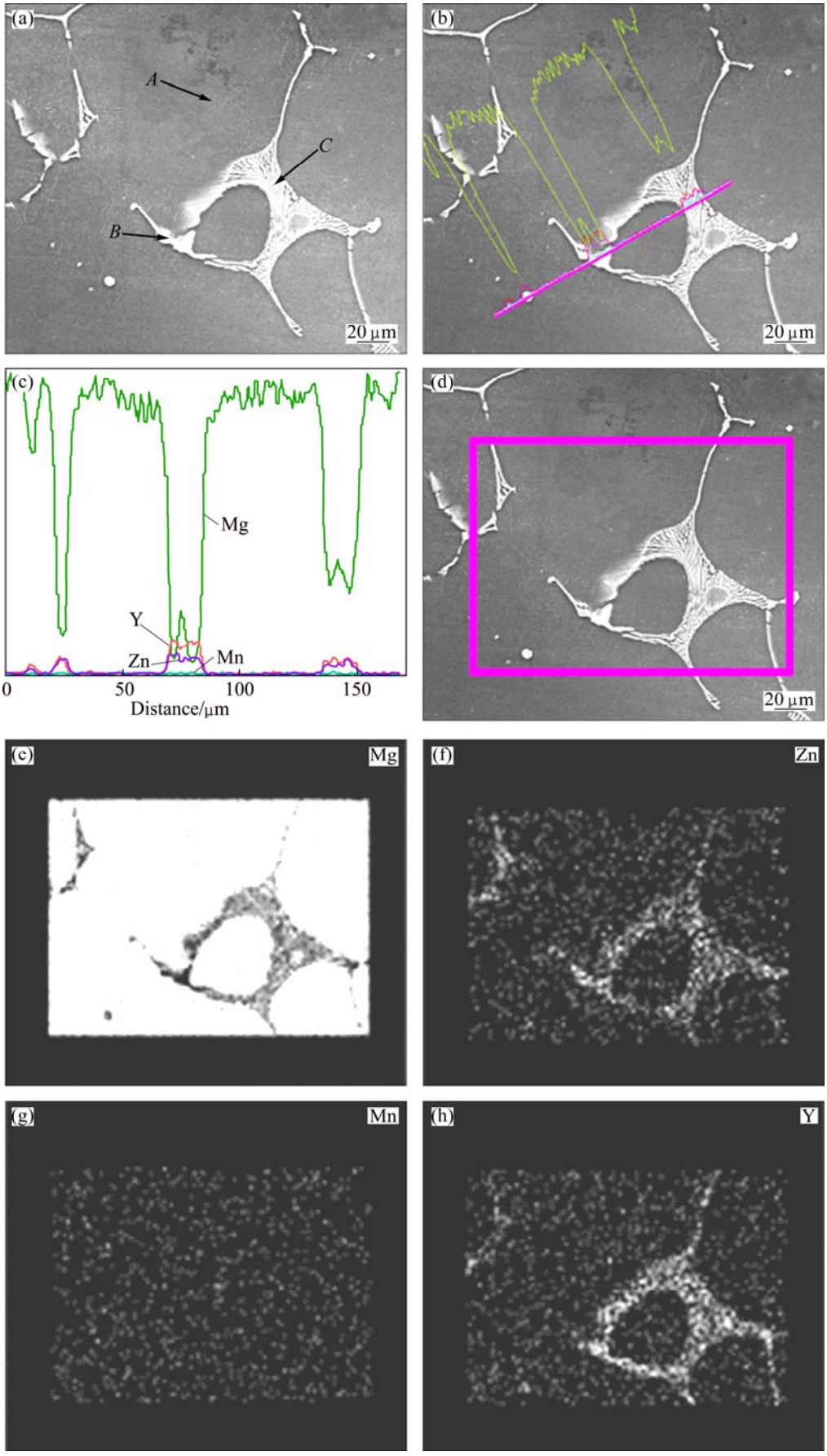

Fig. 4 SE-SEM image and EDS results of as-cast alloy III: (a) EDS spot analysis; (b, c) EDS line scanning; (d−h) EDS mapping

Table 3 EDS results of points *A*, *B* and *C* in Fig. 4(a)

Point	Mole fraction/%				Zn to Y ratio
	Mg	Zn	Mn	Y	
A	98.49	1.16	0.35	0	0
B	85.28	12.43	0.41	1.88	6.61
C	66.97	19.67	0.55	12.81	1.54

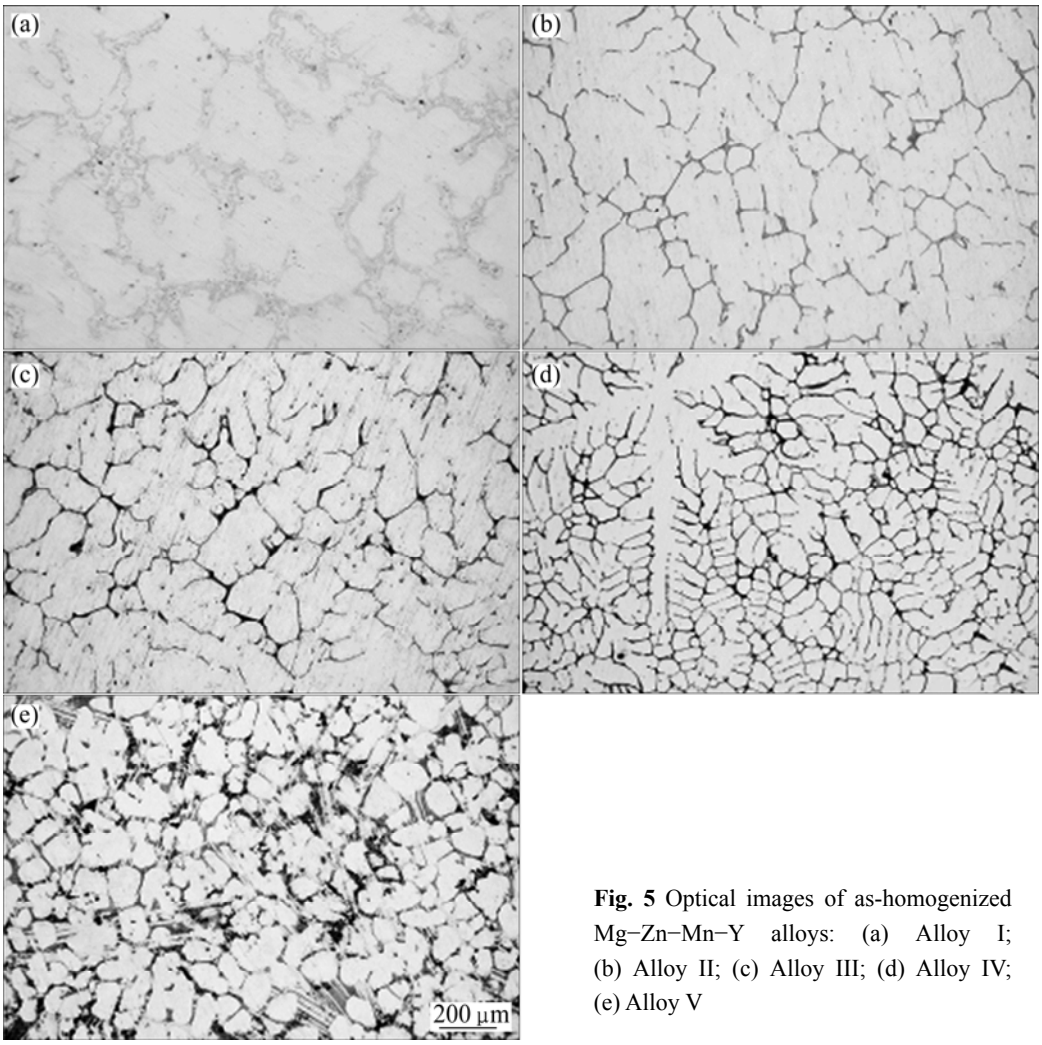

Fig. 5 Optical images of as-homogenized Mg−Zn−Mn−Y alloys: (a) Alloy I; (b) Alloy II; (c) Alloy III; (d) Alloy IV; (e) Alloy V

almost all the eutectic Mg−Zn compounds in the grain boundary can dissolve into the matrix after homogenization treatment at 400 °C for 16 h (Fig. 5(a)). However, for the alloys II−V, almost all the Mg−Zn−Y eutectic phases still remained after the homogenization, as shown in Figs. 5(b)−(e). This implies that Y can increase the thermal stability of the experimental alloy.

Thermodynamic data of the investigated alloys are further determined by DSC analysis shown in Fig. 6. The important thermal parameters are summarized in Table 4. All peaks can be identified in all curves of the samples. The DSC results show that with the variation of Y content, the peaks of the alloys will also change. For the alloy I without Y content, the first peak is located at a temperature of about 348 °C, which is the eutectic temperature of Mg−Zn phases. For the alloy II with a Zn to Y mass ratio of 8.38, the second peak at about 462 °C is absent. With increasing Y content (alloy III), the second and third peaks are observed at about 461 °C and 522 °C, respectively. When the Y content is 3.02% (alloy IV), the second peak disappears and the third peak is at about 528 °C. Based on the XRD results and the previously reports [9,11,20], it can be concluded that the second peak at about 462 °C is the eutectoid melting temperature of *I*-phase, while for the alloys III and IV the third peak at about 522 °C is the eutectic melting temperature of *W*-phase. For the alloy V, two peaks, about 520 °C for *W*-phase and 545 °C for *X*-phase,

should be observed [9,21]. However, only one peak at about 533 °C between 520 °C and 545 °C can be detected before the alloy melts. On one hand, the eutectic melting temperature of *W*-phase is close to that of *X*-phase; on the other hand, the *W*-phase and *X*-phase alternately grow during the solidification process so that the combination of two phases is very good [2]. It can be observed that with increasing Y content, the melting temperature decreases gradually from 634 °C to 615 °C. This shows that solidification temperature range of the experiment alloys greatly reduces, which is very useful for improving the castability of Mg−Zn−Mn−Y alloy. From the DSC study, two conclusions can be obtained: 1) the addition of Y can greatly increase the eutectic temperature of Mg−Zn−Mn alloy; 2) the addition of Y can improve the castability of Mg−Zn−Mn alloy.

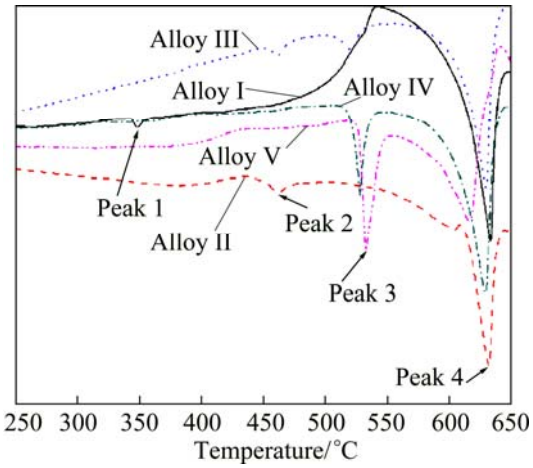

Fig. 6 DSC curves of as-cast Mg−Zn−Mn−Y alloys

To further understand the phase stability of Mg−Zn−Y ternary phases, homogenization treatment at 500 °C for 16 h for alloys III and V was carried out. Figure 7 shows the as-homogenized microstructures of alloys III and V at 400 °C for 16 h and 500 °C for 16 h, respectively. As mentioned before, after homogenization at 400 °C for 16 h, the Mg−Zn−Y eutectic phases including *I*, *W* and *X* phases cannot dissolve into the matrix, as shown in Figs. 7(a) and (c). In contrast, after homogenization at 500 °C for 16 h, *I*-phase can completely dissolve into matrix while only a small part of *W*-phase can dissolve, as shown in Fig. 7(b). However, *X*-phase has no decomposition after homogenization at 500 °C for 16 h, as shown in Fig. 7(d). Based on the thermal analysis and microstructure observation, the phase stability follows the trend: $X>W>I>Mg_7Zn_3$.

3.3 Microstructure of as-extruded alloys

Figure 8 shows the SEM images of extruded Mg−Zn−Mn−Y alloys parallel to the extrusion direction. It shows that the grain size decreases gradually with increasing Y content. As mentioned above, Y has obvious grain refinement effect on the as-cast microstructure of the studied alloys. Moreover, addition of Y initiates the formation of Mg−Zn−Y phases, which can restrain the grain growth effectively during dynamic recrystallization [22]. Figure 8(a) shows the microstructures of the alloy I parallel to the extrusion direction. Equiaxed grain microstructure with the grain size of 14.8 μm is formed owing to the occurrence of dynamic recrystallization (DRX) during the hot extrusion process. When Y content varies from 0 to 0.71%, the grain size of the experiment alloy II decreases, about 10.1 μm. Some eutectic *I*-phases are broken into small particles and move from grain boundaries to grain inside during hot extrusion process. It can be seen that a number of small particles are dispersed in the matrix of alloy II (Fig. 8(b)), which is ascribed to the brittleness of the *I*-phase [9]. Figures 8(c) and (d) are the microstructures of the alloys III and IV. The average grain sizes are about 4.4 and 2.9 μm, respectively. It is clear that the original network distributed secondary phases have been deformed into secondary phase particles along the extrusion direction. When Y content is 6.09%, the grain size is the smallest, only about 1.6 μm. Figures 8 (e) and (f) show that many fine DRX grains form around secondary phase particles and distort grains boundaries in extruded alloy V. However, the DRX process of the alloys III−V is incomplete and the streamline can be observed in the matrix.

Table 4 Data of four DSC peaks in Fig. 6

Alloy	Peak 1		Peak 2		Peak 3		Peak 4	
	t_p/°C	ΔH/(J·g^{-1})	t_p/°C	ΔH/(J·g^{-1})	t_p/°C	ΔH/(J·g^{-1})	t_p/°C	ΔH/(J·g^{-1})
I	348	0.52	−	−	−	−	634	82.77
II	−	−	462	1.36	−	−	632	69.16
III	−	−	461	1.02	522	3.40	630	63.89
IV	−	−	−	−	526	11.11	629	59.52
V	−	−	−	−	533	33.38	615	42.30

ΔH—Heat of phase transformation; t_p—Peak temperature.

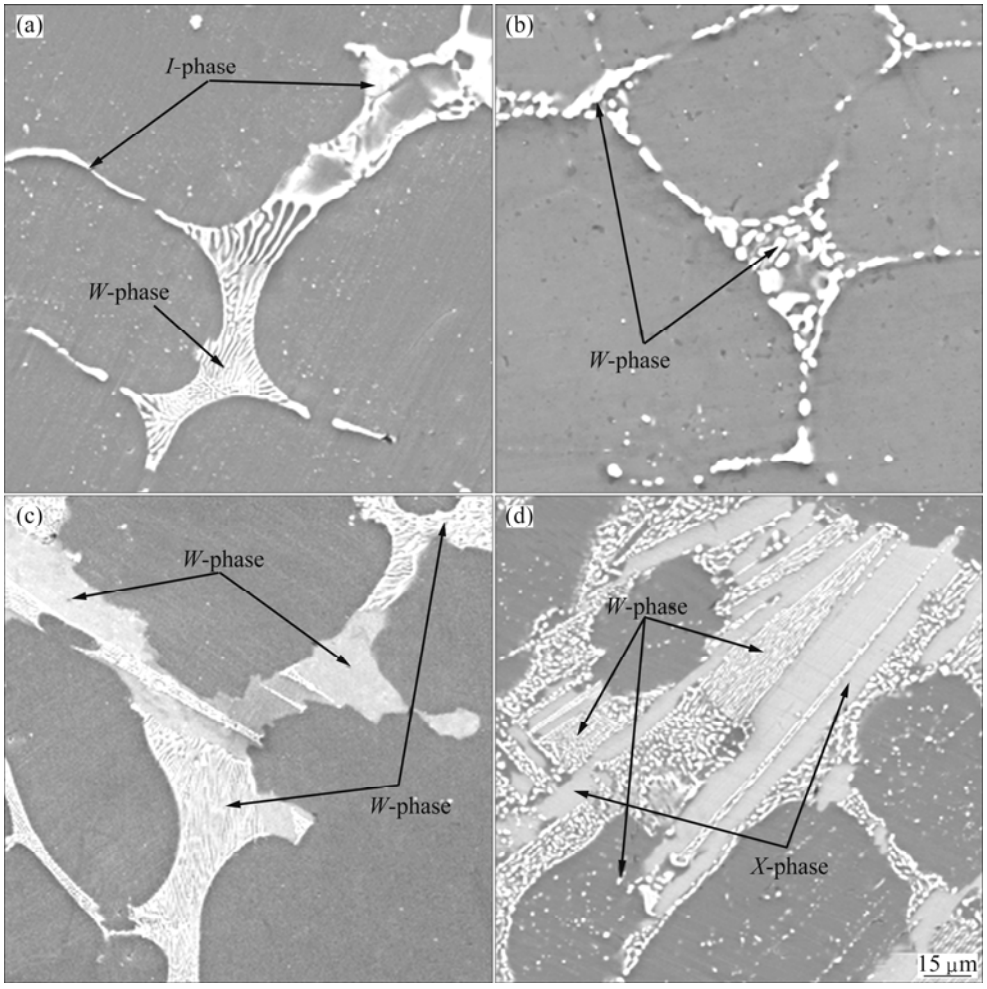

Fig. 7 SE-SEM images of alloy III (a, b) and alloy V (c,d) homogenized at 400 °C (a, c) and 500 °C (b,d) for 16 h

To further illustrate the existence form of Mn element in the extruded alloys, microstructure observation was carried out by TEM. Figure 9 shows a high-angle annular dark-field scanning transmission electron microscopy (HAADF-STEM) micrograph of extruded alloy V and EDS result of a spherical phase particle. EDS result at the "*A*" site further confirms that the spherical particle is the *α*-Mn phase. Based on the XRD analysis and the results in this work, it can be concluded that: 1) Mn has no effect on phase composition. Generally, the ternary equilibrium phases in Mg−Zn−Mn−Y alloy are the same with those in Mg−Zn−Y alloy. 2) Mn element mainly exists as pure Mn particle, which is dispersively distributed in experiment alloys.

3.4 Mechanical properties of as-extruded alloys

The mechanical properties of as-extruded Mg−Zn−Mn−Y alloys are shown in Fig. 10. The results show that with increasing Y content, the strength of the investigated alloy increases obviously while the elongation decreases. For the Y-free alloy (alloy I), the strength is the lowest, but the plasticity is the highest. When the Y content varies from 0 to 3.02%, the strength of the alloy increases gradually. However, there is no difference in the plasticity among the alloys II−IV. When the Y content changes from 3.02% to 6.09%, the strength increases very significantly while the plasticity has a little decrease. Alloy V exhibits the highest tensile ultimate and yield strengths, i.e. 345 MPa and 389 MPa, respectively.

The mechanical properties results show that Y can significantly improve the mechanical properties of the as-extruded Mg−Zn−Mn alloy. The high strengths of Mg−Zn−Mn−Y alloys are mainly due to three aspects: the grain size refinement strengthening, the dispersion strengthening of fine Mn particles, and the introduction of Mg−Zn−Y ternary phases.

As mentioned above, the grain sizes of the as-extruded alloys become much finer with increasing Y contents (Fig. 8). Among them, the grain size of alloy V is the smallest, only about 1.6 μm. The strength of the alloy varies with the grain size and the relationship basically follows the Hall−Petch equation [23].

Apart from the grain refinement strengthening, the size, shape and distribution of Mg−Zn−Y ternary phases

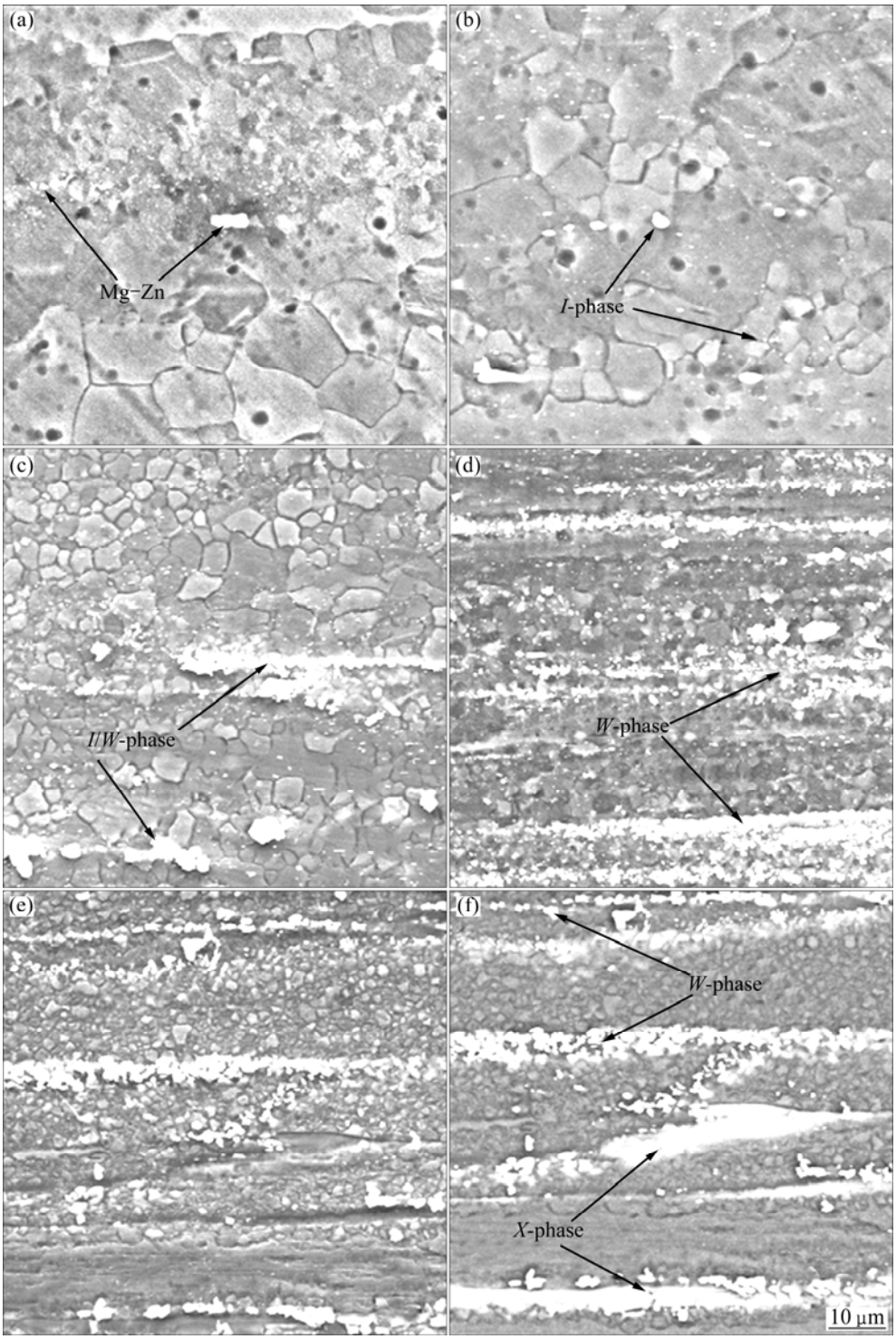

Fig. 8 SE-SEM images (a, b, c, d, e) and BSE-SEM image (f) showing as-extruded microstructures of Mg−Zn−Mn−Y alloys parallel to extrusion direction: (a) Alloy I; (b) Alloy II; (c) Alloy III; (d) Alloy IV; (e), (f) Alloy V

(*I*-phase, *W*-phase and *X*-phase) can also influence the mechanical properties of the alloys. Corresponding to five phase compositions, the phase strengthening effect is as follows:

W+*X* (alloy V)>*W* (alloy IV)>*W*+*I* (alloy III)>
I (alloy II)>$MgZn_2$ (alloy I)

It can be concluded that the strengthening effect of *X*-phase on the Mg−Zn−Mn−Y alloy is more efficient among Mg−Zn−Y ternary phases. It was reported that there is a stable coherent interface between the *X*-phase and the *α*-Mg matrix, which is important for the strength of the alloy [24]. It was previously reported [2,13,25] that the atomic bonding between the *W*-phase and *α*-Mg matrix is very weak and the *W*-phase has no

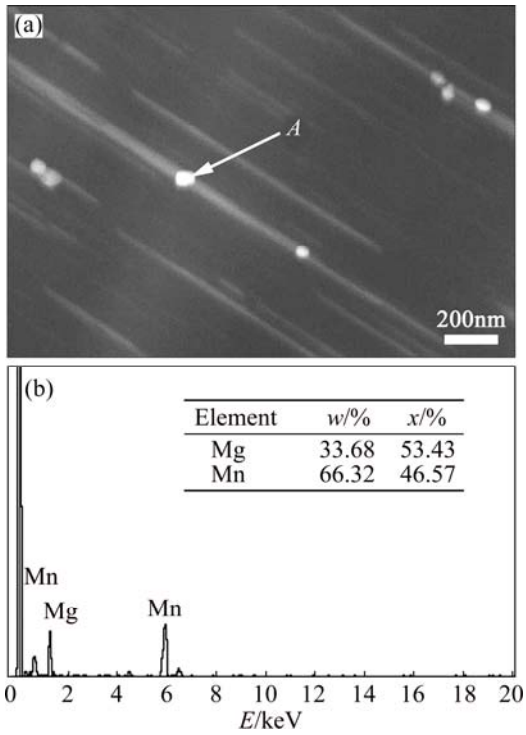

Fig. 9 HAADF-STEM micrograph of extruded alloy V (a) and corresponding EDS results of point *A* (b)

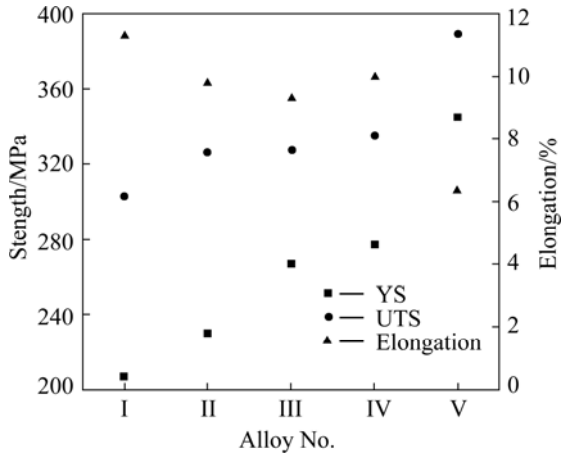

Fig. 10 Mechanical properties of as-extruded Mg−Zn−Mn−Y alloys

conspicuous strengthening and toughening effects on the Mg−Zn−Y−Zr alloys. However, the studied alloy containing *W*-phase can also process good strength and plasticity. On one hand, the dispersive distribution of the *W*-phase after hot extrusion can pin the dislocation and contribute some dispersion strengthening to the studied alloys; on the other hand, the *W*-phase can restrain the grain growth during hot extrusion and contribute some fine grain strengthening to the studied alloys.

In addition, Mn element mainly exists as pure Mn particle, which is dispersively distributed in the experiment alloys. The size of the spherical Mn particle is about 65 nm. It has been reported that Mn element has the function of refining grain size and improving the strengths of magnesium alloys [18,19].

3.5 Fracture analysis

Figure 11 shows the SE-SEM and BSE-SEM images of the tensile fracture surfaces of the experimental alloys with different Y contents machined from cross section of the extruded bars. Figure 12 shows the BSE-SEM microstructures of ruptured samples parallel to the tensile direction.

Figures 11(a) and (b) show the SE-SEM and BSE-SEM fractographs of tensile samples of alloy I, respectively. Huge amounts of plastic dimples are present and some tear ridges can also be observed. The white regions in Fig. 11(b) are the Mg−Zn phases. As shown in Fig. 12(a), a number of fine and parallel twins are observed in the matrix and cracks are initiated and formed at the twins. Figures 11(c) and (d) show the SE-SEM and BSE-SEM images of tensile fracture surface of alloy II. The white particles in Fig. 11(d) are the *I*-phases. It is known that *I*-phase is extremely brittle at room temperature. Therefore, it is easier to deform and evenly distribute during the hot extrusion process [26]. There are many cleavage planes and some tearing ridges to be formed on the fracture surfaces. It can also be found that cracks are also initiated and formed at the twins. Figures 11(e)−(h) show the SEM fractographs of tensile samples of alloy III and IV separately observed by SE and BSE. Some big secondary phases containing mainly *W*-phase apparently increase, as shown in Figs. 11(f) and (h). Due to high hardness of eutectic *W*-phase in as-cast alloy, it is difficult to destroy it during the hot extrusion process. Therefore, the *W*-phase particles are mostly distributed by cluster in the average size range of 4−9 μm. During tensile test, *W*-phase particles are broken and cracked to form micro-cracks, as shown in Figs. 12(c) and (d). Figures 11(i) and (j) show the SEM fracture images of tensile specimen of alloy V observed using SE and BSE, respectively. There are a large number of *W*-phase particles and *X*-phase observed on the fracture surface. As shown in Fig. 12(e), the cracks only initiate at the rupture of *X*-phase. This is due to the fact that *X*-phase and Mg matrix have the axis-to-axis orientation relationship [2,24]. Therefore the strengthening effect of *X* phase is better than *I*-phase or *W*-phase.

Corresponding to five phase compositions, the alloys show different fracture behaviors: for the alloys containing $MgZn_2$ or *I*-phase, the cracks are initiated and formed at the twins and the main crack tends to propagate mostly along deepened twins; for the alloys containing *W*-phase and/or *X*-phase, the cracks form by the fracture of eutectic *W*-phase and/or *X*-phase.

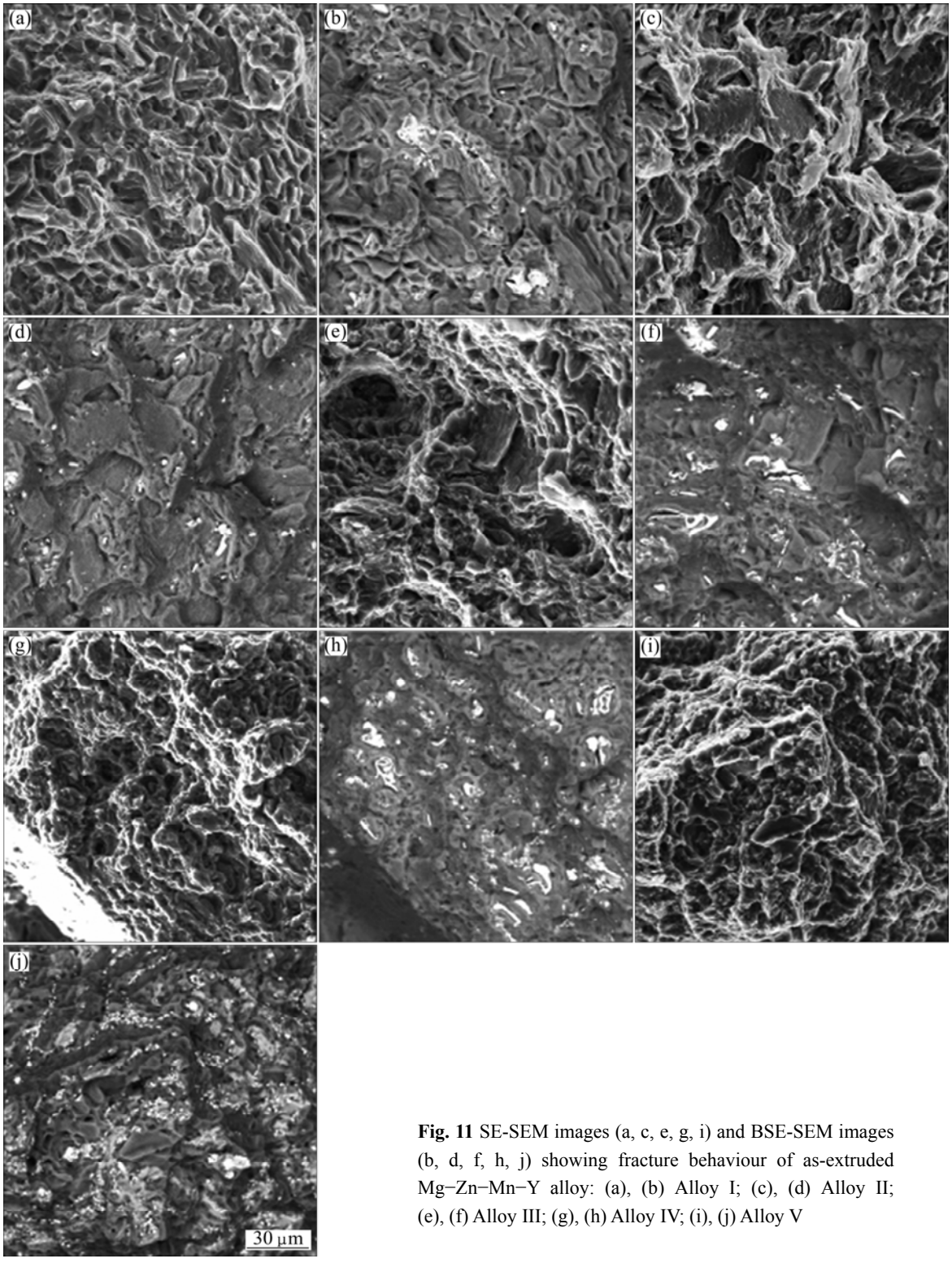

Fig. 11 SE-SEM images (a, c, e, g, i) and BSE-SEM images (b, d, f, h, j) showing fracture behaviour of as-extruded Mg−Zn−Mn−Y alloy: (a), (b) Alloy I; (c), (d) Alloy II; (e), (f) Alloy III; (g), (h) Alloy IV; (i), (j) Alloy V

4 Conclusions

1) The addition of Y has significant effects on the phase composition and microstructure of Mg−6Zn−1Mn alloy. Varied phase compositions, including Mg_7Zn_3, *I*-phase (Mg_3YZn_6), *W*-phase ($Mg_3Y_2Zn_3$) and *X*-phase ($Mg_{12}YZn$), are obtained by adjusting the Zn to Y mass ratio.

2) Mn element has no effect on phase composition and mainly exists as pure Mn fine particles, which are well distributed in Mg−Zn−Mn−Y alloy.

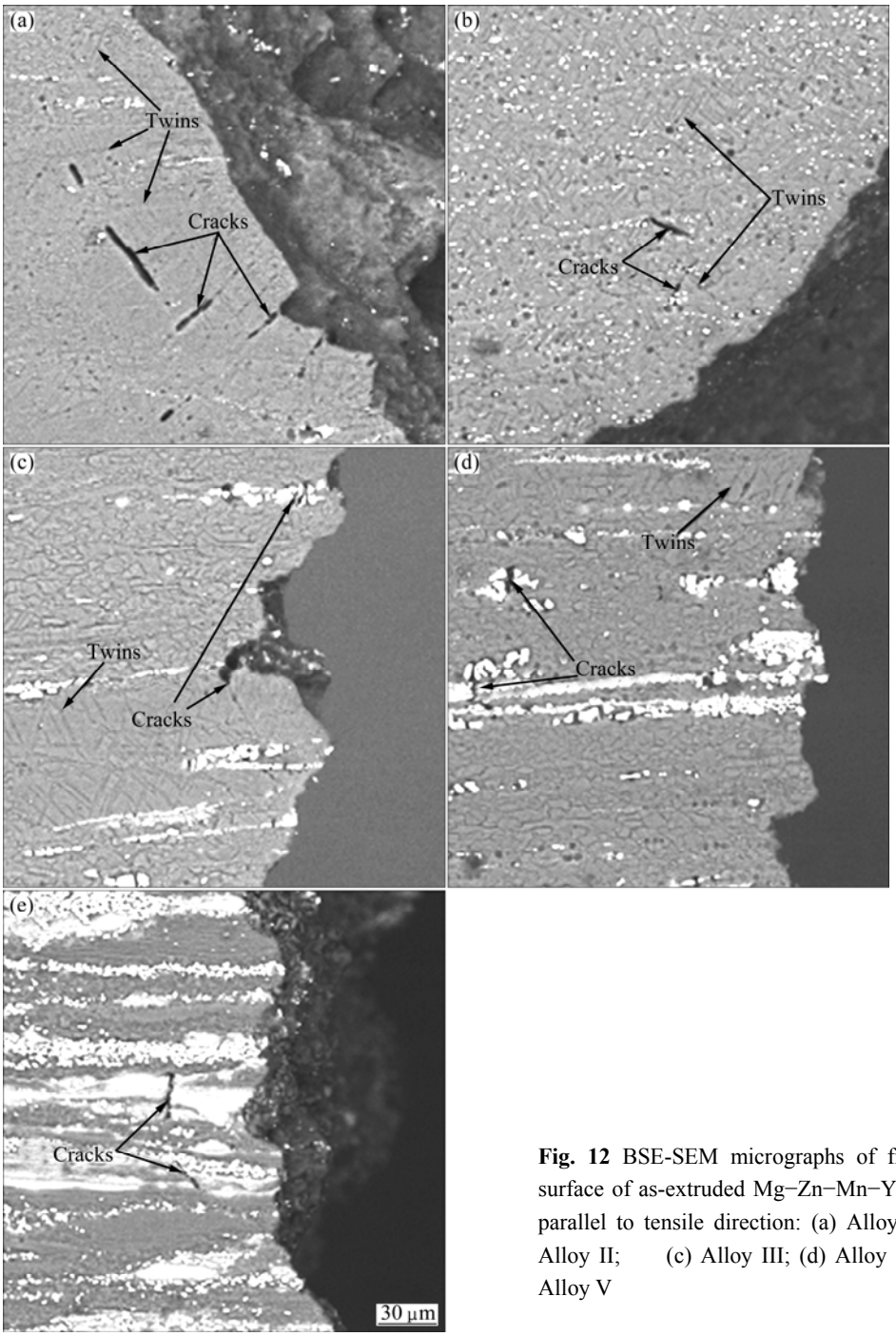

Fig. 12 BSE-SEM micrographs of fracture surface of as-extruded Mg−Zn−Mn−Y alloys parallel to tensile direction: (a) Alloy I; (b) Alloy II; (c) Alloy III; (d) Alloy IV; (e) Alloy V

3) The addition of Y can greatly increase the eutectic temperature of Mg−6Zn−1Mn alloys. Based on the thermal analysis results and microstructure observation, phase stability follows the decrease trend of *X*>*W*>*I*>Mg_7Zn_3.

4) The addition of Y can significantly improve the mechanical properties of Mg−6Zn−1Mn alloy. Among them, the Mg−6Zn−1Mn−6Y with the *X*-phase and *W*-phase alloy has the best mechanical properties, exhibiting the highest tensile strength of 389 MPa, highest yield strength of 345 MPa and elongation of 6.4%. The high strength of the test alloys is mainly due to the strengthening by the grain size refinement, dispersion strengthening by fine Mn particles, and introduction of Mg−Zn−Y ternary phases.

5) Corresponding to different phase compositions, the experimental alloys show different fracture behaviors: for the alloys containing $MgZn_2$ or *I*-phase, the cracks are initiated at the twins and the main crack tends to propagate mostly along deepened twins; for the alloys containing *W*-phase and/or *X*-phase, the cracks form by the fracture of eutectic *W*-phase and/or *X*-phase.

References

[1] ELIEZER D, AGHION E, FROES F H. Magnesium science, technology and applications [J]. Advanced Performance Materials, 1998, 5(3): 201−212.

[2] WANG Jing-feng, GAO Shan, SONG Peng-fei, HUANG Xue-fei, SHI Zhang-zhi, PAN Fu-sheng. Effects of phase composition on the mechanical properties and damping capacities of as-extruded Mg−Zn−Y−Zr alloys [J]. Journal of Alloys and Compounds, 2011, 509(34): 8567−8572.

[3] YANG Z, LI J P, ZHANG J X, LORIMER G W, ROBSON J. Review on research and development of magnesium alloys [J]. Acta Metallurgica Sinica, 2008, 21(5): 313−328.

[4] LUO A A. Recent magnesium alloy development for elevated temperature applications [J]. International Materials Reviews, 2004, 49(1): 13−30.

[5] WU Guo-hua, SUN Ming, WANG Wei, DING Wen-jiang. New research development on purification technology of magnesium alloys [J]. The Chinese Journal of Nonferrous Metals, 2010, 20(6): 1021−1031. (in Chinese)

[6] ZHANG Ding-fei, SHI Guo-liang, DAI Qing-wei, YUAN Wei, DUAN Hong-ling. Microstructures and mechanical properties of high strength Mg−Zn−Mn alloy [J]. Transactions of Nonferrous Metals Society of China, 2008, 18(S1): s59−s63.

[7] DAI Qing-wei, ZHANG Ding-fei, YUAN Wei, SHI Guo-liang, DUAN Hong-ling. Researches on extrusion, microstructure and mechanical properties of new Mg−Zn−Mn alloy [J]. Journal of Materials Engineering, 2008(4): 38−42. (in Chiense)

[8] LI R G, FANG D Q, AN J, LU Y, CAO Z Y, LIU Y B. Comparative studies on the microstructure evolution and fracture behavior between hot-rolled and as-cast $Mg_{96}ZnY_3$ alloys [J]. Materials Characterization, 2009, 60(6): 470−475.

[9] ZHANG Ya, ZENG Xiao-qin, LIU Liu-fa, LU Chen, ZHOU Han-tao, LI Qiang, ZHU Yan-ping. Effects of yttrium on microstructure and mechanical properties of hot-extruded Mg−Zn−Y−Zr alloys [J]. Materials Science and Engineering A, 2004, 373(1−2): 320−327.

[10] BAE D H, KIM S H, KIM W T, KIM D H. High strength Mg−Zn−Y alloy containing quasicrystalline particles [J]. Materials Transactions, 2001, 42(10): 2144−2147.

[11] XU D, HAN E H, LIU L, XU Y. Influence of higher Zn/Y ratio on the microstructure and mechanical properties of Mg−Zn−Y−Zr alloys [J]. Metallurgical and Materials Transactions A, 2009, 40(7): 1727−1740.

[12] KASHEFI N, MAHMUDI R. The microstructure and impression creep behavior of cast AZ80 magnesium alloy with yttrium additions [J]. Materials & Design, 2012, 39: 200−210.

[13] SINGH A, TSAI A P. On the cubic *W* phase and its relationship to the icosahedral phase in Mg−Zn−Y alloys [J]. Scripta Materialia, 2003, 49(2): 143−148.

[14] LUO Su-qin, TANG Ai-tao, PAN Fu-sheng, SONG Kai, WANG Wei-qing. Effect of mole ratio of Y to Zn on phase constituent of Mg−Zn−Zr−Y alloys [J]. Transactions of Nonferrous Metals Society of China, 2011, 21(4): 795−800.

[15] XU D K, LIU L, XU Y B, HAN E H. The influence of element Y on the mechanical properties of the as-extruded Mg−Zn−Y−Zr alloys [J]. Journal of Alloys and Compounds, 2006, 426(1−2): 155−161.

[16] ZHANG Er-lin, HE Wei-wei, DU Hui, YANG Ke. Microstructure, mechanical properties and corrosion properties of Mg−Zn−Y alloys with low Zn content [J]. Materials Science and Engineering A, 2008, 488(1−2): 102−111.

[17] KAWAMURA Y, HAYASHI K, INOUE A, MASUMOTO T. Rapidly solidified powder metallurgy $Mg_{97}Zn_1Y_2$ alloys with excellent tensile yield strength above 600 MPa [J]. Materials Transactions, 2001, 42(7): 1172−1176.

[18] KHAN S A, MIYASHITA Y, MUTOH Y, SAJURI Z B. Influence of Mn content on mechanical properties and fatigue behavior of extruded Mg alloys [J]. Materials Science and Engineering A, 2006, 420(1−2): 315−321.

[19] ZHANG Ding-fei, QI Fu-gang, SHI Guo-liang, DAI Qing-wei. Effects of Mn content on microstructure and mechanical properties of Mg−Zn−Mn wrought alloys [J]. Rare Metal Materials and Engineering, 2010, 39(12): 2205−2210. (in Chinese)

[20] BAE D H, KIM S H, KIM D H, KIM W T. Deformation behavior of Mg−Zn−Y alloys reinforced by icosahedral quasicrystalline particles [J]. Acta Materialia, 2002, 50(9): 2343−2356.

[21] LEE J Y, DO H K, LIM H K, KIM D H. Effects of Zn/Y ratio on microstructure and mechanical properties of Mg−Zn−Y alloys [J]. Materials Letters, 2005, 59(29−30): 3801−3805.

[22] WANG Jing-feng, SONG Peng-fei, GAO Shan, WEI Yi-yun, PAN Fu-sheng. Influence of Y on the phase composition and mechanical properties of as-extruded Mg−Zn−Y−Zr magnesium alloys [J]. Journal of Materials Science, 2012, 47(4): 2005−2010.

[23] HALL E. O. The deformation and ageing of mild steel .3. Discussion of results [J]. Proceedings of the Physical Society of London Section B, 1951, 64(381): 747−753.

[24] SHAO X H, YANG Z Q, MA X L. Strengthening and toughening mechanisms in Mg−Zn−Y alloy with a long period stacking ordered structure [J]. Acta Materialia, 2010, 58(14): 4760−4771.

[25] WANG Y, ZHANG Y, ZENG X, DING W. Characterization of dynamic recrystallisation in as-homogenized Mg−Zn−Y−Zr alloy using processing map [J]. Journal of Materials Science, 2006, 41(12): 3603−3608.

[26] YI S, PARK E S, OK J B, KIM W T, KIM D H. Icosahedral phase+*α*-Mg two phase microstructures in the Mg−Zn−Y ternary system [J]. Materials Science and Engineering A, 2001, 300(1−2): 312−315.

稀土 Y 对 Mg−Zn−Mn 镁合金显微组织和力学性能的影响

齐福刚[1]，张丁非[2]，张孝华[1]，潘复生[2]

1. 中国工程物理研究院 表面物理与化学重点实验室，绵阳 621907；2. 重庆大学 材料科学与工程学院，重庆 400045

摘　要：研究不同稀土 Y 含量对 Mg−6Zn−1Mn 合金显微组织和力学性能的影响。结果表明：Y 元素的添加对 Mg−6Zn−1Mn 合金的相结构、组织和力学性能有明显的影响。随着 Y 含量的增加，合金中的第二相依次从 Mg_7Zn_3 相、*I* 相 (Mg_3YZn_6)、*I* 相+*W* 相 ($Mg_3Y_2Zn_3$)到 *W* 相+*X* 相 ($Mg_{12}YZn$)转变；热分析和组织观察证明合金相的稳定性趋势为 *X* 相>*W* 相>*I* 相>Mg_7Zn_3 相；Mn 元素主要以单质颗粒形式弥散分布在基体中；Y 的添加能显著提升 Mg−Zn−Mn 合金的力学性能，其中含 6.09%Y 的挤压态合金具有最佳的力学性能，其抗拉强度和屈服强度分别达到 389 MPa 和 345 MPa。合金强度的提升主要源于 Y 元素的晶粒细化、Mn 颗粒的弥散强化和 Mg−Zn−Y 稀土相的引入。

关键词：Mg−Zn−Mn 合金；Y；组织；力学性能；断裂

(Edited by Hua YANG)